ORIGINAL RESEARCH

Acute Lung Injury and Fibrosis in a Baboon Model of *Escherichia coli* Sepsis

Ravi S. Keshari[1]*, Robert Silasi-Mansat[1]*, Hua Zhu[1], Narcis I. Popescu[1], Glenn Peer[2], Hala Chaaban[3], John D. Lambris[4], Holly Polf[5], Cristina Lupu[1], Gary Kinasewitz[2], and Florea Lupu[1,6]

[1]Cardiovascular Biology Research Program, Oklahoma Medical Research Foundation, Oklahoma City, Oklahoma; [2]Department of Medicine, Pulmonary and Critical Care Division, [3]Department of Pediatrics, Neonatal and Perinatal Medicine Division, and [6]Departments of Cell Biology and Pathology, University of Oklahoma Health Sciences Center, Oklahoma City, Oklahoma; [4]Department of Pathology and Laboratory Medicine, School of Medicine, University of Pennsylvania, Philadelphia, Pennsylvania; and [5]Oklahoma State University Center for Veterinary Health Sciences, Stillwater, Oklahoma

Abstract

Sepsis-induced inflammation of the lung leads to acute respiratory distress syndrome (ARDS), which may trigger persistent fibrosis. The pathology of ARDS is complex and poorly understood, and the therapeutic approaches are limited. We used a baboon model of *Escherichia coli* sepsis that mimics the complexity of human disease to study the pathophysiology of ARDS. We performed extensive biochemical, histological, and functional analyses to characterize the disease progression and the long-term effects of sepsis on the lung structure and function. Similar to humans, sepsis-induced ARDS in baboons displays an early inflammatory exudative phase, with extensive necrosis. This is followed by a regenerative phase dominated by proliferation of type 2 epithelial cells, expression of epithelial-to-mesenchymal transition markers, myofibroblast migration and proliferation, and collagen synthesis. Baboons that survived sepsis showed persistent inflammation and collagen deposition 6–27 months after the acute episodes. Long-term survivors had almost double the amount of collagen in the lung as compared with age-matched control animals. Immunostaining for procollagens showed persistent active collagen synthesis within the fibroblastic foci and interalveolar septa. Fibroblasts expressed markers of transforming growth factor-β and platelet-derived growth factor signaling, suggesting their potential role as mediators of myofibroblast migration and proliferation, and collagen deposition. In parallel, up-regulation of the inhibitors of extracellular proteases supports a deregulated matrix remodeling that may contribute to fibrosis. The primate model of sepsis-induced ARDS mimics the disease progression in humans, including chronic inflammation and long-lasting fibrosis. This model helps our understanding of the pathophysiology of fibrosis and the testing of new therapies.

Keywords: lung; acute respiratory distress syndrome; sepsis; organ failure; fibrosis

Clinical Relevance

Sepsis-induced acute lung injury and subsequent persistent inflammation are potential triggers of the fibrotic response. We developed a baboon model of sepsis-induced acute respiratory distress syndrome that leads to long-term inflammation and fibrosis and thus recapitulates the pathophysiology of the human disease.

(Received in original form May 13, 2013; accepted in final form September 3, 2013)

*R.S.K. and R.S.-M. contributed equally to this work.

This work was supported by National Institutes of Health grant GM097747-01 (F.L. and J.D.L.).

Author Contributions: G.P., R.S.-M., N.I.P., and H.C. performed the animal experimentation; R.S.-M. performed immunofluorescence analysis and antibody arrays; R.S.K. performed ELISA assays; H.Z. performed quantitative RT-PCR analysis; H.P. performed computed tomography scan imaging; C.L. performed experiments, analyzed results, and contributed to writing the paper; G.K. performed lung compliance tests, analyzed results, and contributed to writing the paper; F.L., J.D.L., and G.K. designed the research; and F.L. supervised the project and wrote the paper.

Correspondence and requests for reprints should be addressed to Florea Lupu, Ph.D., Cardiovascular Biology Research Program, Oklahoma Medical Research Foundation, 825 NE 13th Street, Oklahoma City, OK 73104. E-mail: florea-lupu@omrf.org

This article has an online supplement, which is accessible from this issue's table of contents at www.atsjournals.org

Am J Respir Cell Mol Biol Vol 50, Iss 2, pp 439–450, Feb 2014

Originally Published in Press as DOI: 10.1165/rcmb.2013-0219OC on September 25, 2013
Internet address: www.atsjournals.org

Acute lung injury and the more severe acute respiratory distress syndrome (ARDS) affect almost 190,000 individuals in the United States each year, causing over 75,000 deaths (1). Sepsis is the most common cause of ARDS, accounting for about half of all cases (2). Sepsis-induced ARDS has a complex pathophysiology, driven by excessive inflammatory and coagulopathic responses (reviewed in Ref. 3). The key drivers of the initial exudative phase are microvascular dysfunction and loss of barrier integrity of the endothelial and alveolar epithelial layers (2). The ensuing fibroproliferative repair phase includes the proliferation of type 2 epithelial cells and the local production of new collagen in the lung (4). Many survivors of ARDS have computed tomographic (CT) evidence of pulmonary fibrosis long after their ARDS has clinically resolved (5), and their functional impairment may last even longer (6–9).

Despite the clinical importance of the disease and the extensive research undergone so far, the fundamental mechanisms controlling ARDS progression are not fully defined, no efficient treatments are available, and in-hospital mortality from ARDS remains very high (1, 10). Pathology studies in patients at the onset and during ARDS progression are limited (11), and the information is mainly derived from specimens collected postmortem or, rarely, on open-lung biopsies (12). These studies provided descriptive information and led to the hypothesis that ARDS can cause lung fibrosis (4). However, a clinically relevant animal model is essential to test this hypothesis, because of the multitude of clinical variables that cannot be controlled in critically ill patients. Most of the experimental ARDS models use small animals studied over relatively short periods of time, which may have limited relevance for the human disease (13, 14). Furthermore, many pharmacological studies based on mediators identified in rodent models have failed to provide survival benefits in the clinical trials of humans. The disconnect between outcomes of preclinical and clinical studies could be explained by the lack of a clinically relevant animal model that recapitulates the complexity or biology of the human disease (13, 14). In particular, the determinants of fibrotic proliferation, as well as which factors govern fibrosis resolution during the late stages of the disease, remain poorly understood (15).

Our group has developed and extensively characterized a baboon model of sepsis-induced ARDS by intravenous infusion of live *Escherichia coli* (reviewed in Ref. 16). Here, we used this model to characterize the time course of ARDS progression. We show that our model replicates many responses observed in patients with sepsis-induced ARDS, including an inflammatory stage at 24 hours, fibroproliferative and regenerative phases at 7 days, followed by sustained inflammation and increased extracellular matrix deposition for 6 to 27 months after challenge.

Materials and Methods

Expanded Materials and Methods, including reagents, are contained in the online supplement.

Experimental Model

The study protocol was approved by the Institutional Animal Care and Use Committees of both Oklahoma Medical Research Foundation and the University of Oklahoma Health Science Center. *Papio cynocephalus* baboons (2–3 yr old; 7–10 kg body weight) were infused with 5×10^9 to 2×10^{10} cfu/kg live *E. coli*, as previously described (17).

E. coli–challenged animals were killed after 24–48 hours, corresponding to the exudative phase ARDS ($n = 4$), 7 days (proliferative phase; $n = 6$) or 6–27 months (fibrotic phase; $n = 6$; 2 at 6 mo, 2 at 9 mo, 1 at 12 mo, and 1 at 27 mo after challenge). The control group ($n = 3$) received saline infusion only. Physiologic data (temperature, mean systemic arterial pressure, heart and respiration rate) and blood samples were collected during the time course of the experiment, as previously described (17). No mechanical ventilation was used during the experiment.

Static compliance of the lung was measured in selected animals, as described in the online supplement.

After baboons were killed, lung tissue specimens were snap frozen in liquid nitrogen and stored at −80°C or fixed for microscopy (18).

Histology

Tissue samples were fixed in 10% formalin, embedded in paraffin, and processed for the following specific histological stainings: Masson's trichrome and Picro-Sirius Red (19) for collagen, phosphotungstic acid–hematoxylin for fibrin, and Pearl's Prussian blue for hemosiderin (iron deposits). Histopathologic analysis was done by an experienced veterinary pathologist (Dr. S. Kosanke, University of Oklahoma Health Sciences Center), who was blinded to the experimental conditions.

Immunohistochemistry

For immunofluorescence, tissues were fixed in 4% paraformaldehyde, cryoprotected in 15% sucrose in PBS, embedded in Optimal Cutting Temperature compound, snap frozen, and stored at −80°C.

We used previously described protocols (20) (*see* online supplement) to immunolocalize the following antigens: (*1*) matrix proteins and remodeling enzymes (procollagen 1 and 3, osteopontin and tenascin, and tissue inhibitor of matrix metalloprotease [TIMP] 1); (*2*) signaling mediators (transforming growth factor [TGF]-β, phospho-Smad 2, connective tissue growth factor [CTGF], phospho-platelet-derived growth factor (PDGF) receptor 2, and phospho–mitogen-activated protein kinase [MAPK]); (*3*) markers of apoptosis (active caspase 3), and cell proliferation (Ki67 and proliferating cell nuclear antigen); and (*4*) cell type markers (CD68 for monocyte/macrophages, CD163 for M2 subtype macrophages [21], elastase for neutrophils, α-actin, vimentin, and fibroblast activation protein [FAP] for myofibroblasts); and (*5*) markers of epithelial-to-mesenchymal transition (EMT) (S100A4 and Notch staining in fibroblasts positive for FAP or procollagen 1, and nuclear detection of β-catenin, Snail, and Slug, as Wnt signaling markers) (22).

Electron Microscopy

Tissue samples were fixed with glutaraldehyde and osmium tetraoxide, embedded in epoxy resin, and further prepared and examined as previously described (20).

Biochemical Analysis

See the online supplement for details.

CT Imaging

High-resolution CT scan of the thorax 27 months after challenge in one baboon and scan of a normal age- and weight-matched control baboon for comparison were obtained (*see* the online supplement).

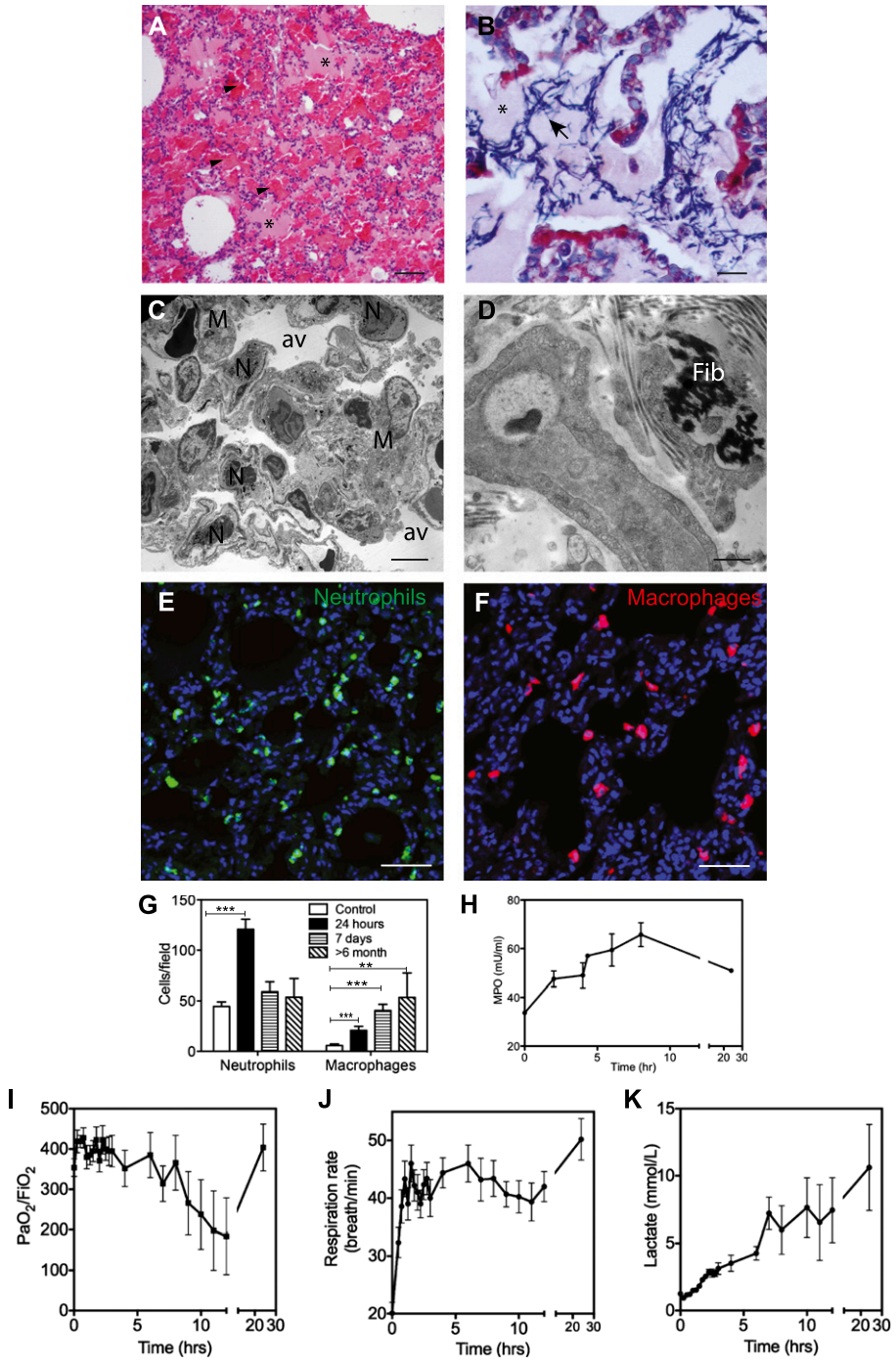

Figure 1. Histological and physiological changes of the lung during the acute exudative phase of acute respiratory distress syndrome (ARDS) in the baboon model of *Escherichia coli* sepsis. (*A* and *B*) Hematoxylin and eosin (*A*) and phosphotungstic acid–hematoxylin (PTAH) (*B*) staining show the presence of protein-rich edema fluid filling the alveoli (*A* and *B*, asterisks), spotty intra-alveolar hemorrhage (*A*, *arrowheads*), and intra-alveolar fibrin deposition (*B*, *blue staining*, *arrows*). (*C* and *D*) Electron micrographs, showing (*C*) neutrophil (N) and macrophage (M) accumulation, and (*D*) the presence of interstitial fibrin (Fib), suggest the activation of coagulation. (*E* and *F*) Immunostaining of elastase-stained neutrophils (*E*) and CD68-positive macrophages (*F*) in the lung of healthy control and septic baboons after 24 hours after challenge. Nuclei are shown in *blue*. (*G*) Quantitation of neutrophils and macrophages in the lung during the time course of the study. Histogram data are shown as means ± SEM (n = 10 microscopic fields collected from at least three different animals per condition per time point; one-way ANOVA with Dunnett's multicomparison test, $^{**}P < 0.01$,

Statistical Analysis

Values are given as means (± SEM). The differences between groups were compared by a two-tailed, unpaired t test or one-way ANOVA, followed by Dunnett's multicomparison test using Prism (GraphPad, LaJolla, CA). Differences were considered significant when P was less than 0.05. All assays were performed at least in duplicate.

Results

Acute Inflammatory Exudative Phase

Our group has developed a baboon model of *E. coli* sepsis that mimics progressive multiple organ failure in humans (16). Baboons challenged with 10^9–10^{10} cfu/kg (lethal dose, 50%) live *E. coli* by intravenous infusion develop ARDS, characterized by robust inflammation, epithelial and endothelial injury, increased permeability, and microthrombosis (Figure 1).

Animals that were killed at 24–48 hours after challenge showed typical features of the exudative phase of ARDS described in humans, characterized by increased permeability of the alveolar–capillary barrier that leads to intra-alveolar hemorrhage, accumulation of protein-rich eosinophilic material (Figure 1A), and fibrin deposition into the alveolar and interstitial compartments, as shown by phosphotungstic acid–hematoxylin staining (Figure 1B) and electron microscopy (Figure 1D). Lung edema and endothelial and epithelial injury are accompanied by a marked activation and influx of neutrophils and mononocytes/macrophages into the interstitium, as shown by quantitative immunostaining for neutrophil elastase (Figures 1E and 1G) and CD68 (Figures 1F and 1G), respectively, as well as electron microscopy (Figure 1C). Leukocyte accumulation in the lung is paralleled by marked decrease of white blood cells in the blood within the first hours after challenge (data not shown) and increased plasma levels of myeloperoxidase, an enzyme released from activated neutrophils (Figure 1H).

The animals showed signs of acute dyspnea and hypoxemia (Figure 1I), including tachypnea (Figure 1J) and tachycardia (data not shown), and increases in plasma lactate levels (Figure 1K). Time course plasma levels of inflammatory cytokines showed steep increases in IL-6, IL-8, and IL-1RA after 2 and 8 hours after challenge (Figure 2). IL-1β and IL-10 increased after 2 hours, dropped at 8 hours, and rebounded later.

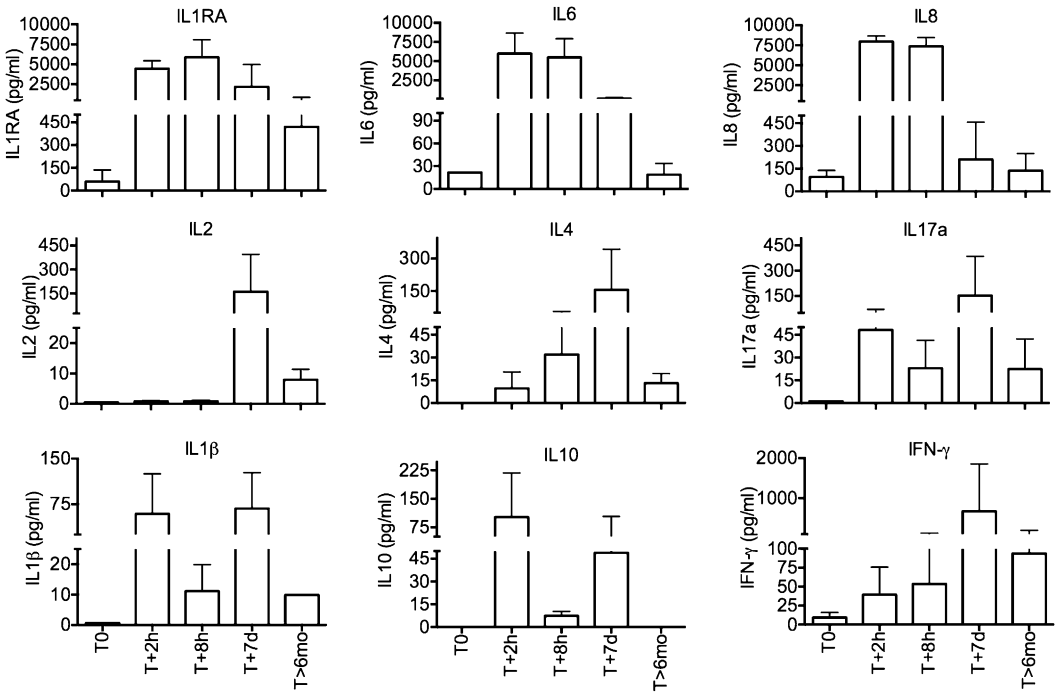

Figure 2. Time course changes of cytokine production during acute sepsis and the long-term follow-up in baboons challenged with *E. coli*. Ethylenediaminetetra-acetic acid plasma samples were collected before challenge (T0), at 2 hours (T + 2 h) and 8 hours (T + 8 h), 7 days (T + 7 d), and 6 months (T + 6 mo) after sepsis challenge. Data are shown as means ± SEM.

Sepsis-induced ARDS triggers cell death. Besides endothelial dysfunction and leukocyte adherence and transvasation, epithelial cells also showed signs of severe damage. Immunostaining for active caspase 3, the major effector enzyme of apoptosis (Figures 3A–3C) and terminal deoxynucleotidyl transferase dUTP nick end labeling staining of fragmented chromatin (Figures 3D–3F) demonstrate strong induction of apoptosis in the lung of septic baboons.

Electron microscopy shows drastic ultrastructural changes of epithelial cells, ranging from cytoplasmic swelling, vacuolization, and bleb formation to necrosis and complete denudation (Figures 3G–3H). Occasionally, chromatin condensation, an ultrastructural feature of apoptosis (23), is observed in cells with epithelial morphology (Figure 3G, *asterisk*).

Proliferative Phase

After 7 days, macrophage infiltration in the lung was significantly increased, whereas the number of neutrophils, although decreased relative to the previous stage, remained slightly higher than in healthy control animals (*see* Figure E1 in the online supplement). Most of the macrophages expressed the M2 subtype marker CD163 (data not shown). Cytokine profiling (Figure 2) showed that early response cytokines, such as IL-6 and IL-8, were decreased as compared with the acute stage; IL-1RA still showed significantly increased levels, whereas IL-2, IL-4, IL-17, and IFN-γ reached their peak at this time point.

Double immunostaining for cytokeratin 18, a type 2 epithelial cell marker, and the cell proliferation marker, Ki67 (Figure 4A), showed extensive staining of epithelial cells from challenged animals as compared with healthy control animals, suggesting that an active reparative process of the alveolar epithelium was taking place. Induction of procollagen-3 and its chaperon, heat shock protein 47, suggests that active collagen synthesis may also occur in cells (presumably myofibroblasts) located within the alveolar wall (Figure 4B). Some collagen-producing myofibroblasts contain S100A4 (fibroblast-specific protein 1, calvasculin), a prototypical marker for EMT (24) (Figure 4C). Codetection of FAP, a protease selectively induced in fibrotic foci (25), together with Notch (Figure 4D) or β-catenin (Figure 4E), two critical signaling proteins that control the EMT phenotype (26, 27), as well as the observed induction of *Snail* + *Slug* transcription factor (Figure 4F), suggest that EMT may play a role in lung fibrogenesis in our model.

Fibrotic Phase

Six animals that survived the acute sepsis challenge were followed for 6–27 months. Although all the animals showed signs of fibrosis after tissue analysis, only one (no. 2,509) had changes in static lung compliance, a pulmonary function test that reflects changes in lung elasticity. This animal had a lung compliance value of 23.1 ml/cm H_2O, which was lower than that measured in five healthy control baboons (median, 35.7 ml/cm H_2O; range, 28.5–45 ml/cm H_2O) that had not been exposed to *E. coli* (Figure 5A). The values did not

Figure 1. (Continued). ***$P < 0.001$). (*H*) Time course changes of plasma myeloperoxidase suggest gradual neutrophil activation and degranulation. (*I–K*) Biochemical and functional tests demonstrate that *E. coli*–challenged baboons showed clinical signs of ARDS: abrupt decrease of blood oxygenation (*I*), increased respiratory rate (tachypnea) (*J*), and gradual increase in plasma lactate (*K*). Data are shown as means ± SEM ($n = 4$). *Scale bars*, 200 μm (*A* and *B*), 10 μm (*C* and *D*), 100 μm (*E* and *F*).

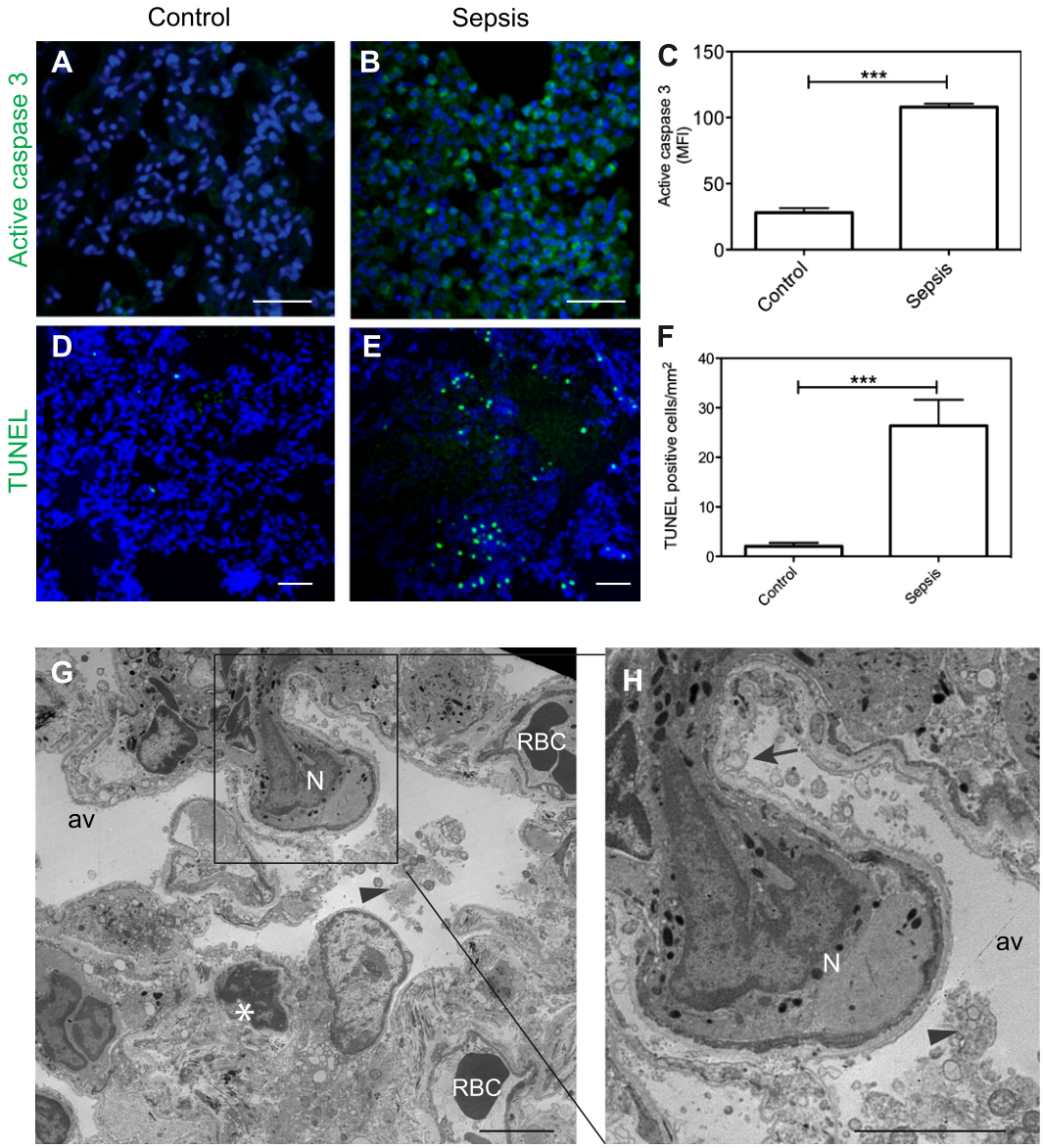

Figure 3. Sepsis-induced cell death in the lung during the first 2 days after *E. coli* challenge in baboons. (*A–F*) Immunofluorescence confocal imaging and quantitative analysis of the lung of healthy control and septic baboons after 24–48 hours after challenge, stained for active caspase 3 (*A–C*; *green*) or DNA fragmentation (terminal deoxynucleotidyl transferase dUTP nick end labeling [TUNEL]; *D–F*; *green*). Nuclei are shown in *blue*. Data are presented as mean ± SEM (n = 10 microscopic fields collected from at least three different animals per condition per time point; unpaired t test, $^{***}P < 0.001$). (*G* and *H*) Electron microscopy images show extensive vacuolization of the type 1 alveolar epithelial cells (*arrow*), intra-alveolar accumulation of cell detritus (*arrowheads*; *G*, *inset* enlarged in *H*). and chromatin condensation in a presumably epithelial cell (*asterisk*). Av, alveolae; N, neutrophil; RBC, red blood cells. *Scale bars*, 100 μm (*A* and *B*), 200 μm (*D* and *E*), 10 μm (*G* and *H*).

correct when the animal was retested after 27 months. Baboon 2,509 was imaged 27 months after *E. coli* challenge using a CT scan, and compared with an age- and weight-matched, nonchallenged animal. In contrast to the control animal (Figure 5C), the challenged animal displayed inhomogeneous lung opacity, as shown on pseudocolor processing (Figure 5B) or densitometry of the gray levels (Figure 5D). These changes were most pronounced peripherally, within the dorsal (posterior) aspect of the lung lobes, and within the caudal (inferior) lung lobes. Changes were bilateral, but were subjectively more severe within the left lung lobes. In the control baboon, mild homogenous attenuation of the lung parenchyma was noted within the dorsal aspect of all lung lobes, consistent with micro atelectasis from dorsal recumbence.

ARDS leads to fibrosis and compromised pulmonary function. Focal fibrosis was detected by Trichrome (Figure 5E) and Sirius red staining (Figures 5F and 5G) in all animals that were killed after 6 months after challenge, but not in healthy control animals. Similarly, procollagens 1 and 3 were strongly expressed in challenged animals as compared with control animals, suggesting active secretion of collagens

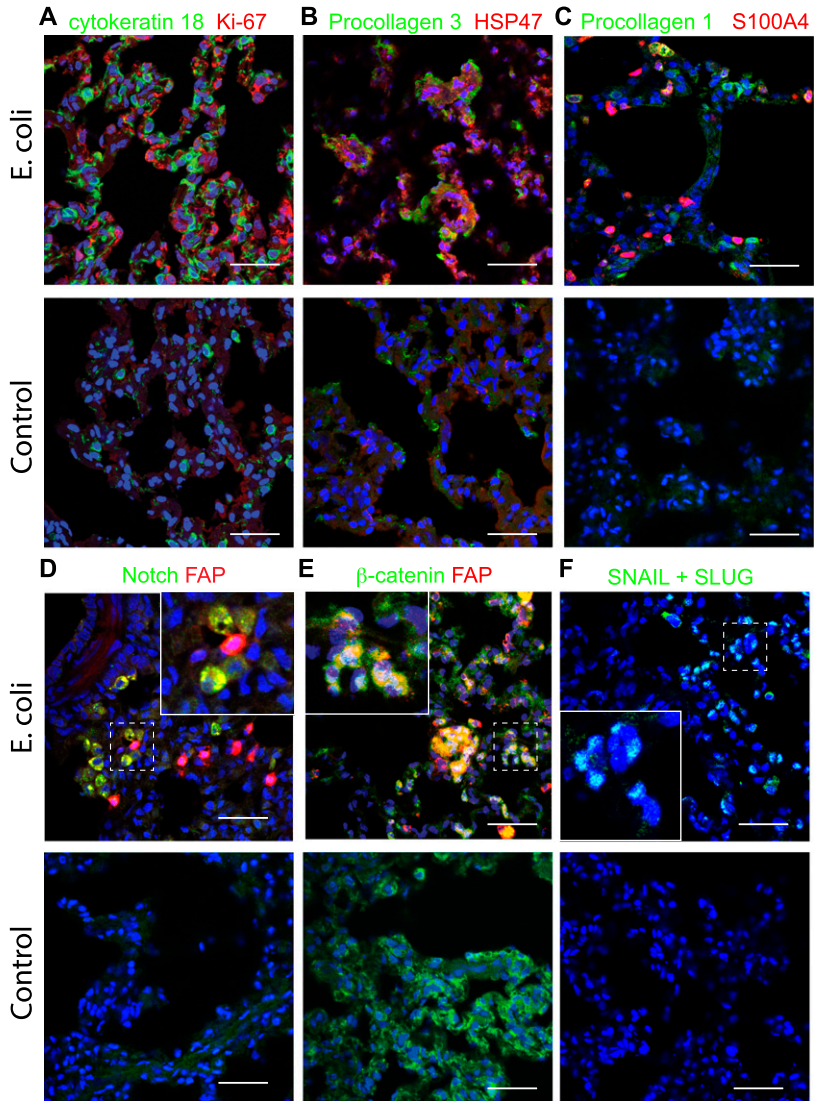

Figure 4. Main pathophysiological features of the lung during the fibroproliferative phase of ARDS after 7 days after *E. coli* challenge. (*A*) Double immunostaining for proliferation marker, Ki67 (*red*), and cytokeratin 18 (*green*, type 2 epithelial cell marker) shows a robust cell proliferation of type 2 epithelial cells in the animals challenged with *E. coli* (*upper row*) versus healthy controls (*lower row*). (*B*) Staining for procollagen 3 using an antibody against the N-terminal domain that detects only the nascent collagen and for chaperon, heat shock protein 47, shows focal induction of collagen synthesis within the lung of septic animals (*upper row*) as compared with healthy control animals (*lower row*). (*C–F*) *E. coli* sepsis induces the expression of markers of epithelial-to-mesenchymal transition: S100A4 (*C*, *red*), Notch (*D*, *green*), β-catenin (*E*, *green*), and SLUG + SNAIL (*F*, *green*). Procollagen 1 (*C*, *green*) or fibroblast activation protein (FAP) (*D* and *E*, *red*) were used as fibroblast markers. High-magnification *insets* of the areas marked with *dashed lines* are shown in (*D–F*). Throughout this figure, nuclei are shown in *blue*. Colocalization of green and red staining is shown as *yellow*; green, red, and blue as *white* (*A–E*), and green and blue as *cyan* (*F*). *Scale bars*, 100 μm.

(Figures 5H and 5I). Because these antibodies are directed toward sites in the NH2-terminal precursor-specific regions of the pro-α1 chains, they detect only the nascent forms of collagens 1 and 3.

Osteopontin, a matrix protein abundantly expressed in the fibrotic lung (28) and potential fibrotic mediator (29, 30), was also detected within the interalveolar septa (Figure 5J). Quantitative RT-PCR (qRT-PCR) showed strong increases in the expression of collagen 1A2 and 3A1 genes (Figure 5K). Quantitation of collagen content in the lung (Figure 5L, healthy controls vs. postchallenge) and procollagen 3 N-terminal peptide in the plasma (Figure 5M, prechallenge vs. postchallenge) showed increased collagen deposition in the animals at over 6 months after challenge as compared with healthy controls or prechallenge values in the same animals. Double staining for myofibroblast markers α-actin and vimentin demonstrates the presence of fibroblastic foci positive for the two markers (data not shown). Electron microscopy confirms the presence of large masses of fibrillar collagen within the alveolar walls of challenged animals (Figures 5N and 5O), but not of control animals (Figure 5P).

Fibroblast proliferation. Staining for phosphorylated MAPK revealed focal activation of MAPK-regulated cell proliferation (Figure E2A). Similarly, staining for two established markers of cell proliferation, Ki67 and proliferating cell nuclear antigen, in conjunction with the fibroblast marker, vimentin (Figures E2B and E2C, and Figures E2D and E2E, respectively), demonstrates ongoing cell proliferation in fibroblastic foci.

Figures E2F and E2G show increased staining for RhoA and Rac, two small GTPases that control cell migration (31), a finding that supports the idea of increased motility of myofibroblasts within the lung interstitium. In contrast, staining of all proteins mentioned previously here was markedly decreased or absent in the lung of healthy control animals.

Persistent inflammation and activation of fibrosis signaling pathways. Quantitative immunostaining for neutrophil and macrophage markers showed significantly increased focal accumulation of macrophages within the lung parenchyma (Figures 1G and 6A–6B) as compared with controls (Figures 1G and 6C), whereas the neutrophils were only slightly affected.

Prussian blue staining showed focal hemosiderosis, which were likely sequels of the intra-alveolar bleeding during the acute exudative stage, and were characterized by accumulation of iron as hemosiderin in the interstitial or alveolar macrophages (Figure 6D).

Most of the macrophages were positive for both CD68 and CD163 (Figure 6E), suggesting that they belong to the M2 subtype. Staining for IL-17 (Figure 6F) showed increased production of this proinflammatory cytokine by cells with macrophage and dendritic cell morphology. Likewise, quantitation of cytokines in

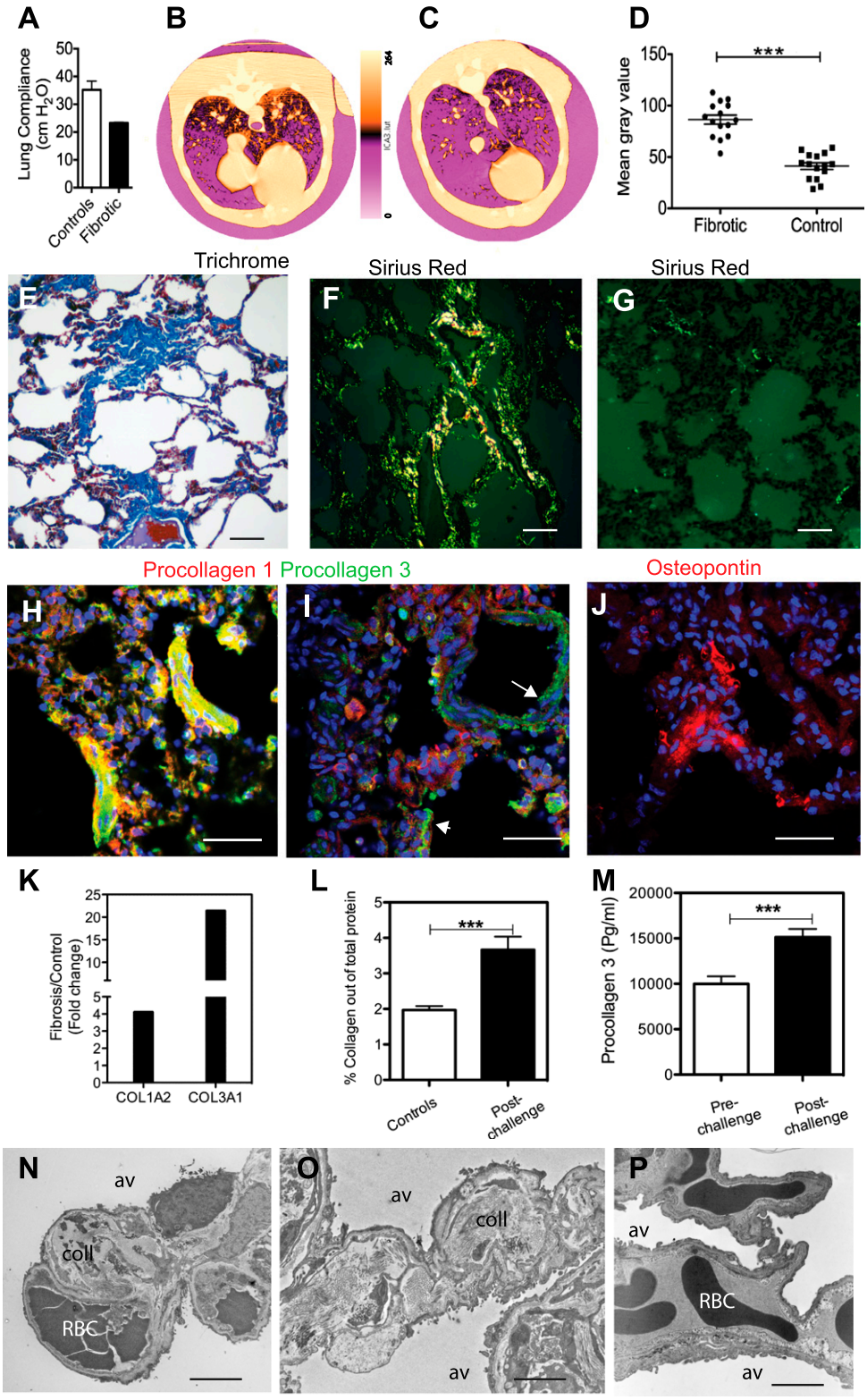

Figure 5. *E. coli* sepsis leads to long-term fibrosis. (*A*) *E. coli* sepsis induces decreased lung elasticity in baboon no. 2,509 that survived 27 months after experimental *E. coli* sepsis as compared with a group of five healthy control animals. This reflects a stiffer organ, as shown by the changes in lung compliance (*C*), expressed as the pressure difference between the interior of the alveoli (P_A) and the pleural cavity (P_{Pl}) (transpulmonary pressure) required to affect a given change in the volume of air (ΔVL) in the lungs ($C = \Delta V_L / \Delta(P_A\text{-}P_{Pl})$). (*B–D*) Pseudocolor-encoded computerized tomography (CT) images of fibrotic lungs from the baboon that survived 27 months after experimental *E. coli* sepsis (*B*) as compared with a healthy control animal (*C*). Changes in

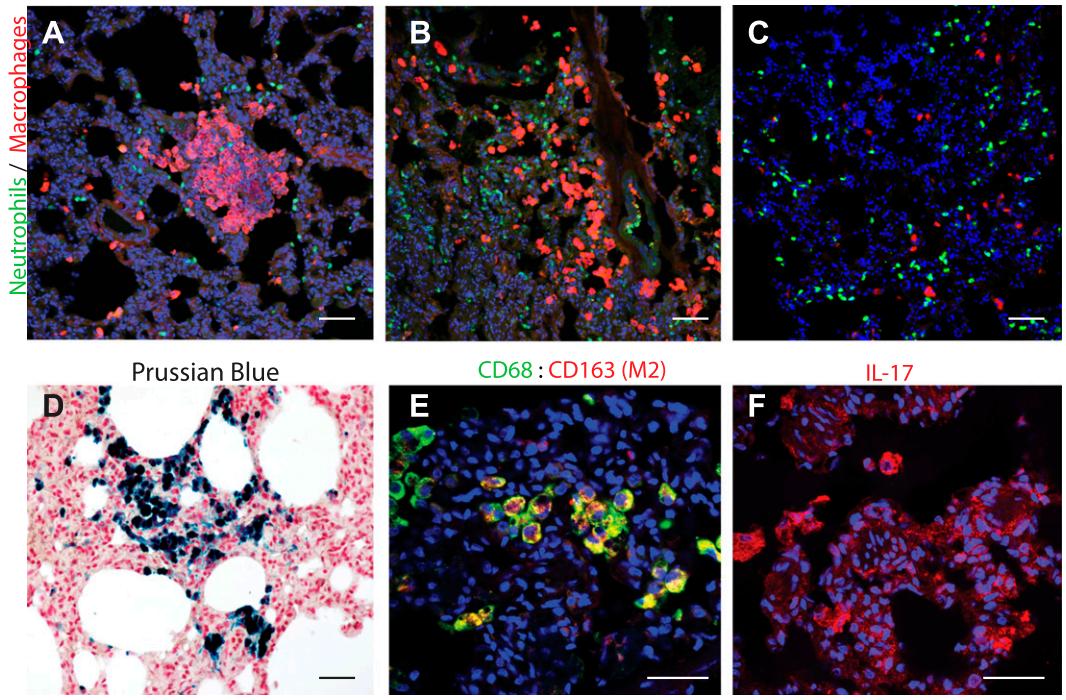

Figure 6. *E. coli* sepsis leads to persistent inflammation in the lung. (*A–C*) Immunostaining for neutrophil elastase (*green*) and macrophage marker, CD68 (*red*), showed significant accumulation of interstitial macrophages in foci within the lung parenchyma (*A*) of an animal killed after 6.5 months (*A*) and 27 months (*B*) after experimental sepsis as compared with a healthy control animal (*C*). The inflammatory infiltrates were frequently associated with the periphery of the organ or with the airway ducts, as shown in (*B*). Quantification of these data is shown in Figure 1G. Although not statistically significant, neutrophil count was also increased, particularly in the areas surrounding macrophage accumulation. (*D*) Staining with Prussian blue showed accumulation of iron-positive (*blue*) hemosiderin-laden macrophages. (*E*) Costaining for CD68 (*green*) and CD163 (*red*; colocalization, *yellow*) suggests that the macrophages accumulated may belong to the M2 subtype. (*F*) Immunostaining for IL-17 shows presence of IL-17–positive cells (*red*) with macrophage morphology. *Scale bars*, 200 μm (*A*, *B*, and *D*), 100 μm (*E* and *F*).

plasma showed that most of the inflammatory cytokines investigated did not return to the initial prechallenge values (Figure 2), further suggesting that persistent inflammation was still ongoing even after over 6 months from the initial lung injury.

Double immunostaining for CD163 and TGF-β (Figures 7A and 7B) showed that the predominant CD163-positive (presumably M2) macrophages could be a source of TGF-β in the lung of these animals. This conclusion is supported by the strong increase in TGF-β1 protein in the plasma after 6–27 months after challenge versus the prechallenge values from the same animals (Figure 7C). FAP, a TNF-induced cell surface serine protease known to associate with reactive fibroblasts (25), was detected in fibroblast foci and in fibrotic interstitium (Figure 7D). Detection by immunostaining of phosphor-Smad2/3 (Figure 7E), a key intracellular mediator of TGF-β profibrotic effects, indicates that active TGF-β signaling was ongoing in FAP-

Figure 5. (Continued). mean gray values in 15 regions-of-interest from three representative CT scan images per experimental condition (fibrotic and control) are shown as a *scatter plot* (*D*). Data are presented as mean ± SEM (two-tailed Student's *t* test; ***$P < 0.001$). (*E–G*) Staining with Mallory's trichrome Masson (*E*; collagen in *blue*) or Sirius red (*F* and *G*; collagen appears as *bright birefringent deposits* under epipolarized light) detects extensive fibrosis within the lung parenchyma (*F*) of challenged baboons, as compared with healthy control animals (*G*). (*H–J*) Staining for procollagen 1 (*H* and *I*, *red*) and 3 (*H* and *I*, *green*), and matrix protein osteopontin (*J*) shows active collagen production and enhanced matrix deposition in the alveolar wall of challenged baboons. Procollagen production in healthy control animals is low and restricted to the adventitia of the large vessels (*I*, *arrow*) or airways (*I*, *arrowhead*). Nuclei are shown in *blue*. Overlay of green and red staining is shown as *yellow*. (*K*) Quantitative RT-PCR (qRT-PCR) of mRNA encoding the collagen 1α2 and collagen 3α1 chains shows strong increased production of these two major matrix proteins in the lung of sepsis survivors as compared with healthy control animals. Data are shown as fold ratio of challenged versus healthy control animals. (*L* and *M*) Biochemical determination of the collagen content of the lung using Sirius red (*L*), represented as percentage of total protein in lung homogenates, shows almost double-fold increase in the baboons that survived sepsis ($n = 6$) versus age matched control animals ($n = 3$). Procollagen 3 activation peptide levels are significantly increased in plasma of the six animals that survived sepsis for over 6 months ($n = 6$), as compared with the plasma of the same animals before experimental sepsis challenge ($n = 6$). Procollagen 3 levels in nonchallenged controls (9,989 ± 923 pg/ml, $n = 3$; not shown on the graph) were not statistically different from the prechallenge values of the experimental groups (10,025 ± 823 pg/ml, $n = 6$). Data are presented as mean ± SEM (two-tailed Student's *t* test; ***$P < 0.001$). (*N–P*) Representative electron micrographs of the lung from an animal that survived sepsis challenge for 6 months (*N* and *O*) show extensive collagen (coll) deposition within the interalveolar walls as compared with a nonchallenged control animal (*P*). av, alveolae; RBC, red blood cells. *Scale bars*, 200 μm (*E–G*), 100 μm (*H–J*), 10 μm (*N* and *O*).

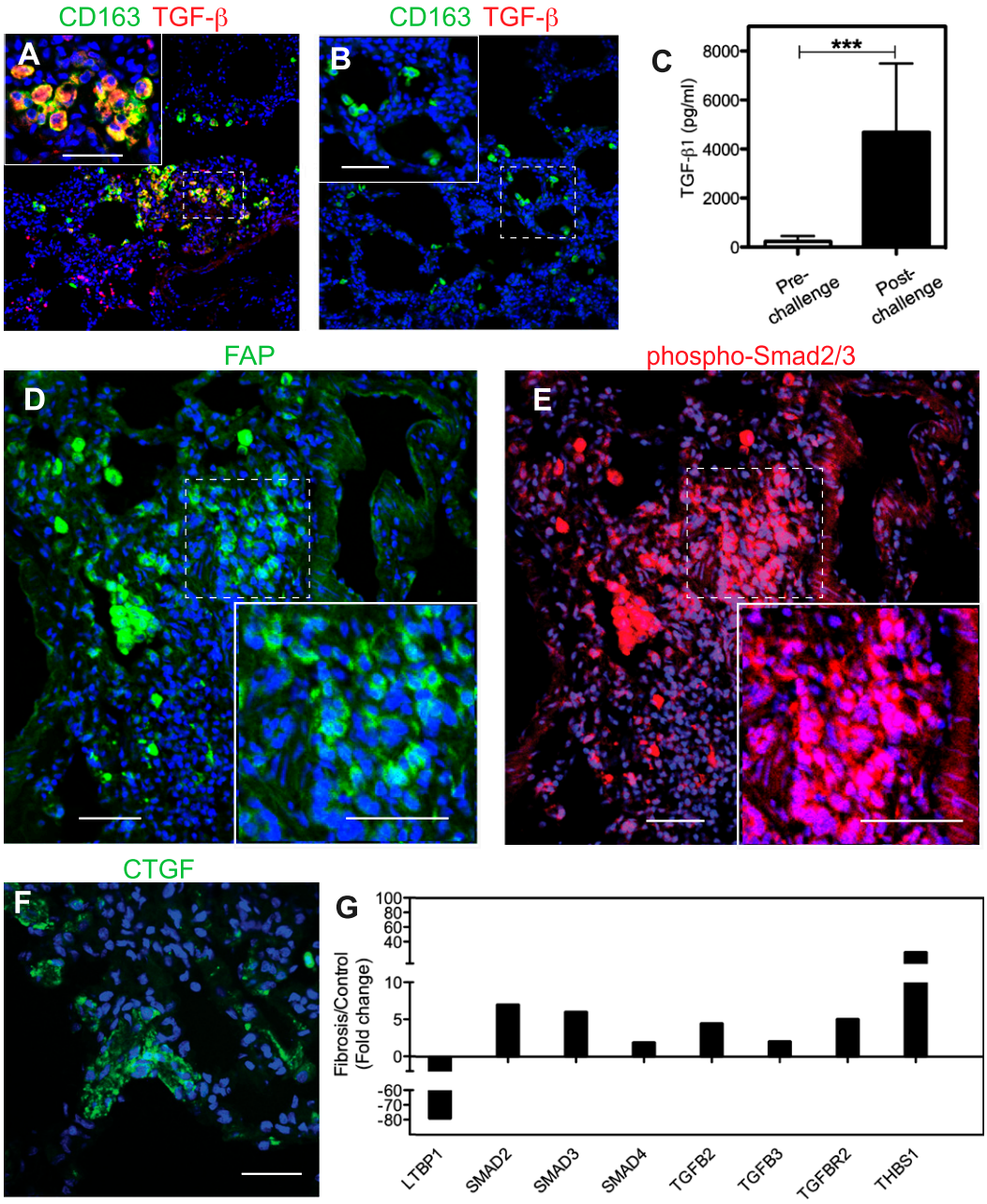

Figure 7. Expression of transforming growth factor (TGF)-β signaling proteins in the lung of long-term sepsis–surviving baboons. (*A* and *B*) Staining for M2 macrophage marker CD163 (*green*) and TGF-β (*red*) in the lung of a baboon killed at 6.5 months after challenge (*A*) shows marked increased accumulation of cells that costain for TGF-β and CD163 (*yellow*; presumably M2 macrophages) in the challenged baboons (*A*) versus unchallenged control animals (*B*). *Insets* show higher magnification of the areas marked with *dashed borders*. Colocalization of the two antigens is shown in *yellow* and nuclei in *blue*. (*C*) Biochemical analysis shows significantly increased TGF-β1 in the plasma of animals that survived *E. coli* sepsis for longer than 6 months as compared with their prechallenge levels. Data are presented as mean ± SEM; 2-tailed Student *t* test; ***$P < 0.001$; $n = 6$ animals. (*D* and *E*) Staining for FAP (*green*; *D*) and phospho-Smad2/3 (*red*; *E*) demonstrates profibrotic TGF-β signaling in activated fibroblasts. Nuclei are shown in *blue*. *Insets* show higher magnification of the areas marked with *dashed borders* to highlight the nuclear staining pattern of phospho-Smad 2/3 (*red* and *blue* overlay appears *purple*). (*F*) Immunostaining for connective tissue growth factor (CTGF; *green*) within the alveolar walls of the lung from a sepsis survivor killed after 6 months after challenge. Lung samples from healthy control animals did not stain for FAP, phospho-Smad, or CTGF (not shown). (*G*) Quantitative RT-PCR analysis shows increased mRNA expression of TGF-β signaling–positive regulators (SMADs 2, 3, and 4, TGF-β, and TGF-β receptor) and thrombospondin 1 (THBS1) transcripts, and down-regulation of the negative regulator, latent TGF-binding protein 1 (LTBP1), in the septic animals killed over 6 months after challenge (fibrosis group) as compared with healthy control animals. Data are shown as average fold change ($n = 6$ animals for fibrosis and $n = 3$ animals for control groups). *Scale bars*, 200 μm (*A*, *B*, *D*, and *E*), 100 μm (*F*).

positive fibroblasts. Moreover, increased immunostaining (Figure 7F) and mRNA expression (Figure E3A) for CTGF, a protein induced by TGF-β and a major mediator of some profibrotic effects of TGF-β (32), were also detected.

qPCR fibrosis pathway–specific assay (Figure 7G) showed increased expression of TGFB2, TGFB3, and receptor, TGFBR2, the intracellular mediators SMAD2, SMAD3, and SMAD4, and thrombospondin-1, an activator of latent TGF-β (33).

Furthermore, qRT-PCR showed strong induction of other profibrotic proteins, including endothelin 1, PDGF-α, and PDGF-β as well as epidermal growth factor receptor (Figure E3A). Along the same line, the plasma PDGF-β level was about twofold increased after 6–10 months after sepsis challenge as compared with the prechallenge values (Figure E3B). Coimmunostaining for phosphorylated PDGF receptor β and α-actin (Figures E3C–E3E) within the alveolar walls suggest active PDGF signaling in fibroblastic foci. In contrast, healthy controls showed staining only in the walls of large vessels or airways.

Besides induction of a robust profibrotic response, the animals that survived sepsis also showed changes in the expression of matrix metalloproteases and TIMPs, suggesting that a decreased matrix turnover may also contribute to the fibrotic process. Thus, TIMPs 1, 2, and 3 mRNA levels were strongly up-regulated (Figure E4A), and plasma TIMP1 was significantly increased in the animals that survived sepsis as compared with their plasma levels before the experimental challenge (Figure E4B). Immunostaining for TIMP1 showed strong focal staining in cells located within the alveolar wall of sepsis survivors (Figure E4C).

Discussion

We have investigated ARDS progression in a nonhuman primate model of *E. coli* sepsis (16). This model recapitulates the main pathophysiological features and consequences of ARDS in humans: an early exudative, inflammatory, and coagulopathic phase, followed by a reparatory fibroproliferative phase that leads to long-term chronic inflammation and fibrosis after 6–10 months. Our model will allow new mechanistic studies on the unknown steps in the transition from sepsis-induced ARDS to lung fibrosis.

Our model recapitulates key pathological changes that occur during acute ARDS in human patients, including severe neutrophil infiltration, intra-alveolar accumulation of protein-rich material, and the formation of microthrombi. In contrast, mouse models intravenously challenged with bacteria (34) show minimal neutrophilic alveolitis and intra-alveolar proteinaceous material. In addition, mice are very resistant to LPS and poorly mimic the inflammation in humans (14), and the changes in alveolar–capillary permeability induced by LPS infusion are mild (13). The profibrotic responses to sepsis observed in baboons resemble, in part, those induced by bleomycin challenge in mice, where the drug triggers acute inflammatory injury followed by reversible fibrosis (35). However, bleomycin challenge does not recapitulate the exudative phase of ARDS (alveolar flooding and proteinaceous material deposition), and the pathophysiological relevance of the challenge is unclear (13). The difference in pathology between mice and primates reflects fundamental differences in anatomy and physiology between these species, such as in the airway architecture and in the alveolar epithelial fluid transport (reviewed in Ref. 36), as well as major interspecies differences in the host immune response to injury (13, 14).

Similar to humans, sepsis-induced ARDS in baboons leads to tachypnea, tachycardia, hypoxemia, and acidosis (3). Histological and ultrastructural analysis showed early loss of the alveolar capillary barrier integrity that results in acute pulmonary edema. Intra-alveolar hemorrhage, flooding of the alveolar space with protein-rich fluid, and deposition of intra-alveolar and interstitial fibrin were observed in animals that were killed within the first 2 days after challenge. Massive influx of inflammatory cells, mainly neutrophils, was paralleled by a steep decrease of leukocytes in the peripheral blood and increase of plasma myeloperoxidase, an enzyme released by activated neutrophils that contributes to oxidative stress and lung injury. Concurrently, epithelial cell injury, leading to apoptosis and necrosis, and sometimes to denudation of the alveolar epithelium, was noticed. These structural changes impair the function of the lung and lead to the severe arterial hypoxemia characteristic of ARDS. These data complement our previous observations (37), as well as unpublished results that suggest that the fibrotic process starts during the first 24 hours after *E. coli* challenge. Our data revealed that, although the early host defense (proinflammatory and procoagulant) responses observed during the first 8 hours are driven by the infused bacteria (38), the genes induced at 24 hours encode mostly profibrotic proteins, including the collagens involved in wound healing, cell proliferation, and extracellular matrix synthesis. The "repair" response suggests that the late stage of sepsis is dominated by a recovery process driven by hypoxia, ischemia, and oxidative stress, triggered by the first stage responses. Our model also mirrors the major late features of human ARDS, the so-called "fibroproliferative" phase (4), characterized by chronic inflammation, proliferation of epithelial cells and myofibroblasts, and sustained matrix synthesis. After 7 days after injury, we observed: (*1*) increased accumulation of CD163-positive (presumably M2 subtype) macrophages that produce regenerative growth factors (39); (*2*) extensive proliferation of alveolar type 2 epithelial cells that further differentiate toward a type 1 phenotype to regenerate the damaged alveolar epithelium; and (*3*) active synthesis and secretion of collagens by fibroblasts, as indicated by staining for procollagen 1 and 3 and their chaperon, heat shock protein 47. Some cells expressed EMT markers, suggesting that a part of the fibroblasts could derive from epithelial cells. However, because our data are based mainly on immunocytochemical staining approaches, we cannot determine the relative contribution of distinct cellular sources and pathways to the fibrosis process in our model. Whereas immunocytochemistry is a versatile tool for detection of specific proteins in tissues, the method has inherent limitations related to tissue preparation, antibody specificity, and the sensitivity of the detection system (40).

We have performed the semiquantitative measurements of fluorescence intensity or integration of stained areas using standardized image analysis methods and rigor of execution to limit the effects of subjective factors (20, 41).

We further investigated the long-term effects of ARDS in animals that survived the acute challenge. We observed persistent matrix synthesis and fibrosis in all animals killed after 6 months after challenge. One

animal showed altered lung compliance and increased X-ray opacity on CT scan images after 27 months after challenge, indicating clinical lung fibrosis. Accumulation of myofibroblasts, coupled with increased collagen production and deposition within the airways and alveolar septa, were documented by microscopy and biochemical assays. The detection of inflammatory cytokines in the systemic circulation, as well as of areas focally enriched in macrophages and other cell types that actively produced IL-17, demonstrates that chronic inflammation still persists long after the initial challenge. CD163-positive (presumably M2) macrophages appeared to contribute to the production of TGF-β, the master regulator of fibrosis (42), but it is likely that the increased TGF-β detected has multiple sources. Detection of the phosphorylated form of Smad2 (43), a major intracellular mediator of TGF-β signaling, and of CTGF, a profibrotic growth factor that acts downstream of TGF-β (44), strongly suggests a major role for this growth factor in the pathogenesis of post-ARDS fibrosis in baboons. Similarly, patients with persistent ARDS after septic shock also display increased circulating TGF-β1 levels (45). Furthermore, patients with ARDS with fatal outcome show higher TGF-β1 concentrations than the survivors (45). These results suggest that high TGF-β1 levels play a relevant role in the pathogenesis of persistent sepsis-induced ARDS (46).

Besides the induction of TGF-β–controlled genes, qRT-PCR analysis showed increased expression of other known profibrotic factors, including endothelin-1, PDGF, and epidermal growth factor receptor, strongly supporting the presence of ongoing fibrosis.

In addition to these known markers of fibrosis, we also observed impaired expression of the proteins involved in the regulation of matrix remodeling. Notably, we found increased production of the TIMPs, suggesting that dysfunctional matrix remodeling may also contribute to the onset and progression of the observed fibrosis. Altered matrix remodeling represents a novel route to fibrosis after sepsis-induced ARDS that can be studied in our model.

To our knowledge, the present study is the first report on the long-term effects of post-ARDS fibrosis in a clinically relevant animal model of gram-negative sepsis. The changes reported here mimic the ARDS progression in a subset of human patients, where the alveolar injury induced by the initial sepsis does not resolve, leading to "late ARDS," a condition characterized by chronic inflammation, fibrotic scaring, and impaired lung function, as well as unfavorable outcome (6, 47). Analysis of open-lung biopsy specimens from patients with late ARDS showed the presence of active fibroproliferative responses and diffuse alveolar damage (47). It has been reported that alveolar fibrosis is present in most patients dying from ARDS, suggesting that fibrosis contributes to the poor outcome (48) and decreased quality of life and quality-adjusted survival (49). We have shown here that young, previously healthy baboons challenged with sepsis ARDS can develop early and persistent fibroproliferative activity that may contribute to long-lasting fibrotic sequels. Similarly, Herridge and colleagues (9) recently reported that relatively young, previously healthy patients who survived ARDS had persistent exercise limitations and a reduced physical quality of life 5 years after their critical illness. Although mechanical ventilation is often a life-saving intervention in ARDS, the procedure can lead to complications, including damage of the alveolae and airways that can exacerbate the fibroproliferative activity in the lung (2). Because we did not use mechanical ventilation of the animals, the persistent inflammation and fibroproliferation observed were likely induced by the early lung injury in response to the infused bacteria, without the superimposed effect of ventilation.

Although we have observed biomarker evidence of increased fibrosis in all six baboons, only one had decreased lung compliance. The higher incidence of fibrosis in our model versus human patients probably reflects the greater sensitivity of immunohistochemical measurements compared with physiological assessment. Moreover, survivors of sepsis-induced ARDS have a lower rate of functional recovery than survivors of other types of ARDS (46).

Our model closely mimics the progression of ARDS and its fibrotic complications in humans, and provides a powerful tool to study the pathogenesis of fibrotic lung disease and to test novel therapies. ■

Author disclosures are available with the text of this article at www.atsjournals.org.

Acknowledgments: The authors thank Dr. Fletcher Taylor for thoughtful advice on the animal model and Dr. Mark Coggeshall for critical reading of the manuscript.

References

1. Rubenfeld GD, Caldwell E, Peabody E, Weaver J, Martin DP, Neff M, Stern EJ, Hudson LD. Incidence and outcomes of acute lung injury. *N Engl J Med* 2005;353:1685–1693.
2. Matthay MA, Ware LB, Zimmerman GA. The acute respiratory distress syndrome. *J Clin Invest* 2012;122:2731–2740.
3. Matthay MA, Zemans RL. The acute respiratory distress syndrome: pathogenesis and treatment. *Annu Rev Pathol* 2011;6:147–163.
4. Meduri GU, Eltorky M, Winer-Muram HT. The fibroproliferative phase of late adult respiratory distress syndrome. *Semin Respir Infect* 1995;10: 154–175.
5. Nobauer-Huhmann IM, Eibenberger K, Schaefer-Prokop C, Steltzer H, Schlick W, Strasser K, Fridrich P, Herold CJ. Changes in lung parenchyma after acute respiratory distress syndrome (ARDS): assessment with high-resolution computed tomography. *Eur Radiol* 2001;11:2436–2443.
6. Heyland DK, Groll D, Caeser M. Survivors of acute respiratory distress syndrome: relationship between pulmonary dysfunction and long-term health-related quality of life. *Crit Care Med* 2005; 33:1549–1556.
7. Needham DM, Dinglas VD, Bienvenu OJ, Colantuoni E, Wozniak AW, Rice TW, Hopkins RO; NIH NHLBI ARDS Network. One year outcomes in patients with acute lung injury randomised to initial trophic or full enteral feeding: prospective follow-up of EDEN randomised trial. *BMJ* 2013;346:f1532.
8. Burnham EL, Janssen WJ, Riches DW, Moss M, Downey GP. The fibroproliferative response in ARDS: mechanisms and clinical significance. *Eur Respir J* (In press)
9. Herridge MS, Tansey CM, Matte A, Tomlinson G, Diaz-Granados N, Cooper A, Guest CB, Mazer CD, Mehta S, Stewart TE, *et al.*; Canadian Critical Care Trials Group. Functional disability 5 years after acute respiratory distress syndrome. *N Engl J Med* 2011; 364:1293–1304.

10. Phua J, Badia JR, Adhikari NK, Friedrich JO, Fowler RA, Singh JM, Scales DC, Stather DR, Li A, Jones A, *et al*. Has mortality from acute respiratory distress syndrome decreased over time? A systematic review. *Am J Respir Crit Care Med* 2009;179:220–227.
11. Capelozzi VL. What have anatomic and pathologic studies taught us about acute lung injury and acute respiratory distress syndrome? *Curr Opin Crit Care* 2008;14:56–63.
12. Donati SY, Papazian L. Role of open-lung biopsy in acute respiratory distress syndrome. *Curr Opin Crit Care* 2008;14:75–79.
13. Matute-Bello G, Frevert CW, Martin TR. Animal models of acute lung injury. *Am J Physiol Lung Cell Mol Physiol* 2008;295: L379–L399.
14. Seok J, Warren HS, Cuenca AG, Mindrinos MN, Baker HV, Xu W, Richards DR, McDonald-Smith GP, Gao H, Hennessy L, *et al*.; Inflammation and Host Response to Injury, Large Scale Collaborative Research Program. Genomic responses in mouse models poorly mimic human inflammatory diseases. *Proc Natl Acad Sci USA* 2013; 110:3507–3512.
15. Marshall R, Bellingan G, Laurent G. The acute respiratory distress syndrome: fibrosis in the fast lane. *Thorax* 1998;53:815–817.
16. Taylor FB Jr, Kinasewitz GT, Lupu F. Pathophysiology, staging and therapy of severe sepsis in baboon models. *J Cell Mol Med* 2012;16: 672–682.
17. Silasi-Mansat R, Zhu H, Popescu NI, Peer G, Sfyroera G, Magotti P, Ivanciu L, Lupu C, Mollnes TE, Taylor FB, *et al*. Complement inhibition decreases the procoagulant response and confers organ protection in a baboon model of *Escherichia coli* sepsis. *Blood* 2010; 116:1002–1010.
18. Tang H, Ivanciu L, Popescu N, Peer G, Hack E, Lupu C, Taylor FB Jr, Lupu F. Sepsis-induced coagulation in the baboon lung is associated with decreased tissue factor pathway inhibitor. *Am J Pathol* 2007;171:1066–1077.
19. Junqueira LC, Bignolas G, Brentani RR. Picrosirius staining plus polarization microscopy, a specific method for collagen detection in tissue sections. *Histochem J* 1979;11:447–455.
20. Lupu C, Westmuckett AD, Peer G, Ivanciu L, Zhu H, Taylor FB Jr, Lupu F. Tissue factor–dependent coagulation is preferentially up-regulated within arterial branching areas in a baboon model of *Escherichia coli* sepsis. *Am J Pathol* 2005;167:1161–1172.
21. Mantovani A, Sica A, Sozzani S, Allavena P, Vecchi A, Locati M. The chemokine system in diverse forms of macrophage activation and polarization. *Trends Immunol* 2004;25:677–686.
22. Haslehurst AM, Koti M, Dharsee M, Nuin P, Evans K, Geraci J, Childs T, Chen J, Li J, Weberpals J, *et al*. EMT transcription factors Snail and Slug directly contribute to cisplatin resistance in ovarian cancer. *BMC Cancer* 2012;12:91.
23. Krysko DV, Vanden Berghe T, D'Herde K, Vandenabeele P. Apoptosis and necrosis: detection, discrimination and phagocytosis. *Methods* 2008;44:205–221.
24. Schneider M, Hansen JL, Sheikh SP. S100a4: a common mediator of epithelial–mesenchymal transition, fibrosis and regeneration in diseases? *J Mol Med* 2008;86:507–522.
25. Acharya PS, Zukas A, Chandan V, Katzenstein AL, Pure E. Fibroblast activation protein: a serine protease expressed at the remodeling interface in idiopathic pulmonary fibrosis. *Hum Pathol* 2006;37: 352–360.
26. Aoyagi-Ikeda K, Maeno T, Matsui H, Ueno M, Hara K, Aoki Y, Aoki F, Shimizu T, Doi H, Kawai-Kowase K, *et al*. Notch induces myofibroblast differentiation of alveolar epithelial cells via transforming growth factor-β–Smad3 pathway. *Am J Respir Cell Mol Biol* 2011;45:136–144.
27. Charbonney E, Speight P, Masszi A, Nakano H, Kapus A. Beta-catenin and Smad3 regulate the activity and stability of myocardin-related transcription factor during epithelial–myofibroblast transition. *Mol Biol Cell* 2011;22:4472–4485.
28. O'Regan A. The role of osteopontin in lung disease. *Cytokine Growth Factor Rev* 2003;14:479–488.
29. Takahashi F, Takahashi K, Okazaki T, Maeda K, Ienaga H, Maeda M, Kon S, Uede T, Fukuchi Y. Role of osteopontin in the pathogenesis of bleomycin-induced pulmonary fibrosis. *Am J Respir Cell Mol Biol* 2001;24:264–271.
30. Pardo A, Gibson K, Cisneros J, Richards TJ, Yang Y, Becerril C, Yousem S, Herrera I, Ruiz V, Selman M, *et al*. Up-regulation and profibrotic role of osteopontin in human idiopathic pulmonary fibrosis. *PLoS Med* 2005;2:e251.
31. Cai GQ, Zheng A, Tang Q, White ES, Chou CF, Gladson CL, Olman MA, Ding Q. Downregulation of Fak-related non-kinase mediates the migratory phenotype of human fibrotic lung fibroblasts. *Exp Cell Res* 2010;316:1600–1609.
32. Abreu JG, Ketpura NI, Reversade B, De Robertis EM. Connective-tissue growth factor (CTGF) modulates cell signalling by BMP and TGF-beta. *Nat Cell Biol* 2002;4:599–604.
33. Murphy-Ullrich JE, Poczatek M. Activation of latent TGF-beta by thrombospondin-1: mechanisms and physiology. *Cytokine Growth Factor Rev* 2000;11:59–69.
34. Cross AS, Opal SM, Sadoff JC, Gemski P. Choice of bacteria in animal models of sepsis. *Infect Immun* 1993;61:2741–2747.
35. Moore BB, Lawson WE, Oury TD, Sisson TH, Raghavendran K, Hogaboam CM. Animal models of fibrotic lung disease. *Am J Respir Cell Mol Biol* 2013;49:167–179.
36. Plopper CG, Hyde DM. The non-human primate as a model for studying COPD and asthma. *Pulm Pharmacol Ther* 2008;21:755–766.
37. Zhu H, Tang Y, Ivanciu L, Centola M, Lupu C, Taylor FB Jr, Lupu F. Temporal dynamics of gene expression in the lung in a baboon model of *E. coli* sepsis. *BMC Genomics* 2007;8:58.
38. Taylor FB Jr. Staging of the pathophysiologic responses of the primate microvasculature to *Escherichia coli* and endotoxin: examination of the elements of the compensated response and their links to the corresponding uncompensated lethal variants. *Crit Care Med* 2001; 29:S78–S89.
39. Mantovani A, Biswas SK, Galdiero MR, Sica A, Locati M. Macrophage plasticity and polarization in tissue repair and remodelling. *J Pathol* 2013;229:176–185.
40. Fritschy JM. Is my antibody-staining specific? How to deal with pitfalls of immunohistochemistry. *Eur J Neurosci* 2008;28:2365–2370.
41. Taylor CR, Levenson RM. Quantification of immunohistochemistry—issues concerning methods, utility and semiquantitative assessment II. *Histopathology* 2006;49:411–424.
42. Alber A, Howie SE, Wallace WA, Hirani N. The role of macrophages in healing the wounded lung. *Int J Exp Pathol* 2012;93:243–251.
43. Tatler AL, Jenkins G. TGF-β activation and lung fibrosis. *Proc Am Thorac Soc* 2012;9:130–136.
44. Wang Q, Usinger W, Nichols B, Gray J, Xu L, Seeley TW, Brenner M, Guo G, Zhang W, Oliver N, *et al*. Cooperative interaction of CTGF and TGF-beta in animal models of fibrotic disease. *Fibrogenesis Tissue Repair* 2011;4:4.
45. de Pablo R, Monserrat J, Reyes E, Diaz D, Rodriguez-Zapata M, la Hera A, Prieto A, Alvarez-Mon M. Sepsis-induced acute respiratory distress syndrome with fatal outcome is associated to increased serum transforming growth factor beta-1 levels. *Eur J Intern Med* 2012;23: 358–362.
46. McHugh LG, Milberg JA, Whitcomb ME, Schoene RB, Maunder RJ, Hudson LD. Recovery of function in survivors of the acute respiratory distress syndrome. *Am J Respir Crit Care Med* 1994;150:90–94.
47. Meduri GU, Belenchia JM, Estes RJ, Wunderink RG, el Torky M, Leeper KV Jr. Fibroproliferative phase of ARDS: clinical findings and effects of corticosteroids. *Chest* 1991;100:943–952.
48. Martin C, Papazian L, Payan MJ, Saux P, Gouin F. Pulmonary fibrosis correlates with outcome in adult respiratory distress syndrome: a study in mechanically ventilated patients. *Chest* 1995;107:196–200.
49. Angus DC, Musthafa AA, Clermont G, Griffin MF, Linde-Zwirble WT, Dremsizov TT, Pinsky MR. Quality-adjusted survival in the first year after the acute respiratory distress syndrome. *Am J Respir Crit Care Med* 2001;163:1389–1394.